Table S3: primer sequences for PCR analysis, related to Figure 1-4.

primer name	Sequences (5' to 3')
NANOG	CCA AAG GCA AAC AAC CCA CTT
	GAC CGG GAC CTT GTC TTC CT
GAPDH	ACC ACA GTC CAT GCC ATC AC
	TCC ACC ACC CTG TTG CTG TA
total *OCT3/4*	CCC CAG GGC CCC ATT TTG GTA CC
	ACC TCA GTT TGA ATG CAT GGG AGA GC
transgene *OCT3/4*	CAT TCA AAC TGA GGT AAG GG
	TAG CGT AAA AGG AGC AAC ATA G
total *SOX2*	TTC ACA TGT CCC AGC ACT ACC AGA
	TCA CAT GTG TGA GAG GGG CAG TGT GC
transgene *SOX2*	TTC ACA TGT CCC AGC ACT ACC AGA
	TTT GTT TGA CAG GAG CGA CAA T
total *L-MYC*	GCG AAC CCA AGA CCC AGG CCT GCT CC
	CAG GGG GTC TGC TCG CAC CGT GAT G
transgene *L-MYC*	GGC TGA GAA GAG GAT GGC TAC
	TTT GTT TGA CAG GAG CGA CAA T
SMN-FL	CAAAAAGAAGGAAGGTGCTCACATT
	GTGTCATTTAGTGCTGCTCTATGC
SMN-⊿7	CTTGATGATGCTGATGCTTTGGGAAG
	CTATGCCAGCATTTCCATATAATAGCCAG
GAPDH	GTGGACCTGACCTGCCGTCT
	GGAGGAGTGGGTGTCGCTGT
Myh3	TGAGATTGCAGGATCTGGTGG
	CTCATGCTGGGCTTTCCTGA
Myh8	GCCGGGAGGTTCACACCAAA
	AAACCCAGAGAGGCAAGTGA

Supplementary experimental procedures

Study approval

Use of human ESCs was approved by the Ministry of Education, Culture, Sports, Science and Technology of Japan (MEXT). The study plan for recombinant DNA research has been approved by recombinant DNA experiments safety committee of Kyoto University. An experimental protocol was approved by the Animal Research Committee of Center for iPS cell research and application, Kyoto University.

Cell lines

The following fibroblasts were obtained from the NIGMS Human Genetic Cell Repository at the Coriell Institute for Medical Research: [GM00232, GM03813]. Donors of both fibroblasts were described as having SMA type I. The iPSCs generated from the GM00232 and GM03813 fibroblasts were renamed CiRA00070 and CiRA00069, respectively, according to the institutional regulations. A human embryonic stem cell line, KhES1, was kindly provided by Dr. Hirofumi Suemori (Institute for Frontier Medical Sciences, Kyoto University, Kyoto, Japan). The human iPS cell lines, 201B7 and 409B2, were kindly provided by Dr. Shinya Yamanaka (Center for iPS Cell Research and Application, Kyoto University, Kyoto, Japan). The murine myoblast cell line, C2C12, was kindly provided by Dr. Atsuko Sehara-Fujisawa (Institute for Frontier Medical Sciences, Kyoto University, Kyoto, Japan).

Establishment of iPSCs

Episomal vectors encoding reprogramming factors (*OCT3/4, SOX2, KLF4, L-MYC, LIN28* and p53 shRNA) were transduced into fibroblasts on day 0 as described previously (Okita et al., 2011). Plasmids were kindly provided by Dr. Keisuke Okita (CiRA, Kyoto University).The transfected cells were reseeded onto feeder layers on day 7, and maintained in embryonic stem cell medium (ReproCELL). Around day 30, the iPSC colonies were picked up as usual.

RNA isolation and quantitative PCR

Total RNA extraction from cells was performed using the RNeasy Mini kit (QIAGEN). One microgram of total RNA was used for reverse transcription with the PrimeScript RT Master Mix (TaKaRa). The real-time PCR was performed with SYBR Premix Ex TaqII (TaKaRa) in triplicate using the StepOnePlus system (Applied Biosystems). *GAPDH* was used as an endogenous control. The primer sets used for the quantitative PCR assay are described in **Table S3**.

Teratoma formation

The iPSCs recovered from one 6 cm dish were injected subcutaneously into NOG mice (Central Institute for Experimental Animals). Tumors were dissected eight weeks after injection and were fixed with PBS containing 4% paraformaldehyde. Paraffin-embedded tissues were sliced and stained with hematoxylin and eosin. Slides were examined using a BIOREVO BZ-9000 system (KEYENCE).

Genotyping (PCR-RFLP)

The methods used to detect homozygous *SMN1* exon 7 and 8 deletions were described previously (van der Steege et al., 1995). In brief, the restriction enzymes Dra I and Dde I cleave the PCR products originating only from *SMN2*, enabling *SMN1*-derived PCR products to be distinguished from those of *SMN2*. The completely

digested band corresponds to the deletion of exons 7 or 8 in *SMN1*. The results of the PCR electrophoresis were analyzed by a bioanalyzer (Agilent)(Burrell et al., 2011).

Protein isolation and Western blot analysis

Cells were isolated, suspended in M-PER (Thermo SCIENTIFIC), supplemented with 1% protease inhibitor cocktail (Sigma) and centrifuged at 20,000 g for 15 min at 4°C. A total of 3.125 µg of protein extracted from each sample was separated on 10% SDS-polyacrylamide gels, transferred to a nitrocellulose membrane, probed with a primary antibody against SMN (1:20,000; BD #610647), followed by horseradish-peroxidase-conjugated secondary antibody (1:10,000; Cell Signaling), and then visualized using ECL chemiluminescence reagents (Amersham). As a control, membranes were stripped and re-probed for β-actin (1:1,000; Cell Signaling #4970S). Quantitative densitometry analysis was performed using ImageQuant LAS 4000 software.

Immunocytochemistry and microscopy

Cells were fixed and permeabilized for 30 min at room temperature in 4% paraformaldehyde and 0.2% TritonX-100, and incubated with Block Ace (DS PHARMA BIOMEDICAL) to prevent any non-specific binding before overnight incubation with primary antibodies at 4°C. The following day, secondary antibody incubations were performed for 1 hour with the appropriate species-specific antiserum coupled to either FITC, Cy3 (Jackson ImmunoResearch, 1/100) or Alexa594 conjugated α-bungarotoxin (α-BTX) (Invitrogen #B13423, 1/500). After staining nuclei with DAPI (1/1,000), the cells were mounted utilizing Vectashield (Vector laboratories) and imaged using a LV1000 confocal microscope (Olympus). All antibodies were diluted in Block Ace. The following primary antibodies were used at the indicated concentrations: neurofilament 160 kDa (Millipore #MAB5254, 1/1000), Tuj1 (Covance #MMS435P, 1/2000), MAP2 (Sigma #M2320, 1/1000), HB9 (DSHB #81.5C10, 1/100), ChAT (Millipore #AB144P, 1/200), anti-synaptic vesicle protein 2 (DSHB #SV2, 1/20), NF-H (abcam #ab4680, 1/5000), mAb35 (DSHB #mAb35, 1:1,000), MHC (Millipore #A4.1025, 1:1,000) and TUNEL (Promega, DeadEnd Fluorometric TUNEL System).

Quantification of the results of the immunocytochemical analysis

Samples were imaged under identical gain and exposure settings. Only motor neurons containing a nucleus were counted in order to avoid double counting from adjoining sections. To calculate the average number of HB9-positive motor neurons, 12 visual fields in each preparation from each condition were counted using the BIOREVO BZ-9000 system (KEYENCE).

For the co-cultured samples, eight visual fields were evaluated and assessed in each preparation. Images were obtained with a 10×objective lens. For measurements, individual images of AChR clusters were imported into the ImageJ software program and split into red (endplate) and green (neurite and motor nerve terminal) channels. Each endplate and corresponding motor nerve terminal was automatically outlined and calculated using the IN Cell Analyzer 2000 software program (GE Healthcare Life Sciences), and areas greater than 427 pixels were kept as targets.

Microarray

Total RNA was extracted and purified using RNA mini kit (QIAGEN) according to manufacturer's instruction. Gene expression analysis was performed using SurePrint G3 Human Gene Expression 8 × 60K kit (G4851A; Agilent technologies). Cy3-labelled cDNA was synthesized from 100 ng of RNA using Genomic DNA Enzymatic Labeling

Kit (Agilent Technologies). Labelled cDNA was fragmented with Gene Expression Hybridization Kit (Agilent Technologies), followed by hybridization at 65˚C for 17 hrs. Images were acquired by DNA Microarray Scanner (Agilent Technologies). The data were normalized by 75 percentile shift using the GeneSpring GX 12.6.1 software (Agilent Technologies). Principle component analysis (PCA) was performed by R ver 3.1.0. Two-way hierarchical clustering analysis was performed using Ward's method based on Euclidean distance. Heatmap was illustrated by GeneSpring GX 12.6.1 using average method based on Euclidean distance.

DNA methylation analysis

Genomic DNA was extracted and purified using PureLink Genomic DNA Mini Kit (Invitrogen) according to manufacturer's instruction. One μg of genomic DNA was subjected to bisulfite conversion of unmethylated cytosines of genomic DNA into uracils with EZ DNA Methylation Gold Kit (ZYMO Research). Promoter regions of *POU5F1* and *NANOG* were amplified by PCR from approximately 10 ng of bisulfite-treated DNA using Ex-taq (TaKaRa). PCR condition for *POU5F1* promoter was: 1 cycle of 98°C for 1 min, followed by 45 cycles of 98°C for 10 s, 60°C for 30 s, and 72°C for 1 min. That for *NANOG* promoter was: 1 cycle of 95°C for 3 min, followed by 40 cycles of 95°C for 30s, 58°C for 30 s, and 72°C for 1 min. Primers were: GTTTTTAGAGTAGTTGGGATTATAG and AACCCACCCTTATAAATTCTCAATTA for *NANOG*; ATTTGTTTTTTGGGTAGTTAAAGGT and CCAACTATCTTCATCTTAATAACATCC for *POU5F1*. Illumina libraries were generated by NEBNext Ultra DNA Library Prep Kit (New England BioLabs), and sequenced in 250 cycles Paired-end mode of MiSeq. All sequence reads were extracted in FASTQ format using MiSeq Reporter v2.3.32. Mapping to canonical sequence of human genome (hg19) was performed by bismark v.0.7.7 (Krueger and Andrews, 2011).

RNA-seq

After depletion of ribosomal RNA by RiboZero Gold (Epicentre), we prepared libraries using the Illumina TruSeq Stranded Total RNA Sample Prep kit. The libraries were sequenced in 100 cycle Single-Read mode of HiSeq2500. All sequence reads were extracted in FASTQ format using BCL2FASTQ Conversion Software 1.8.4 in the CASAVA 1.8.2 pipeline. The sequence reads were mapped to hg19 reference genes, downloaded on 10th December 2012, using Tophat v2.0.8b (Kim et al., 2013) and quantified by RPKMforGenes (Ramskold et al., 2009), downloaded on 19th, October 2012. Gene Ontology analysis was used by David v6.7 (Huang da et al., 2009).

GSE accession numbers

Microarray and RNA-seq deposited in GEO database can be accessed with the GEO accession number GSE65470 and GSE65508, respectively.

Motor neuron differentiation and co-culture with C2C12

The iPSCs were dissociated into single cells and quickly re-aggregated in DFK 5% medium (DMEM/F12 medium supplemented with KSR, NEAA, 2-mercaptoethanol, L-Glutamate, SB431542, dorsomorphin and Y27632) (9000 cells/150 μl/well) using 96-well low cell-adhesion plates (Lipidure-coat U96w from Nunc)(Eiraku et al., 2008; Morizane et al., 2011) . From day 8, the cell aggregates were treated with Sonic hedgehog (100 ng/ml) and retinoic acid (1 μM) for 1 week (Wada et al., 2009). On day 20, the cell aggregates were plated onto poly-l-lysin/laminin-coated culture dishes in neurobasal medium (Gibco) supplemented with the neurotrophic factors GDNF, BDNF and NT3 (10 ng/ml, R & D Systems). The medium was changed every 3-4 days thereafter.

For the co-culture with neuronal cells, the fusion of C2C12 myoblasts was induced by switching to the differentiation medium (DMEM supplemented with horse serum). On day 4, the MNs that had differentiated from the iPSCs (differentiation days 34-54) were harvested and plated on the induced myotubes, and the medium was changed to Neurobasal medium containing neurotrophic factors (BDNF, GDNF, NT3; 10 ng/ml each). Thereafter, the cultures were fed every two days by changing half of the medium.

VPA treatment

Co-cultured samples were treated with or without 1 mM VPA by changing half of the medium every two days. After six days of drug treatment, the area of NF and αBTX immunostaining was detected by immunocytochemistry and was analyzed by the IN Cell Analyzer 2000 software program.

PMO treatment

Designed PMOs SMN2E7D(-10-29) for suppressing splice silencing motifs in intron 7 of *SMN2* (Mitrpant et al., 2013) and its negative control were purchased from GENE TOOLS. SMN- or Ctrl-PMO (10 μM in medium) were introduced with the Endo-Porter (GENE TOOLS) on day 1 of co-culturing, and the cells were subsequently cultured for three days.

Statistics. Statistic functions in Microsoft Excel 2013 was used for statistical analyses. Results are expressed as mean ± SEM. Statistical significance was determined using Student's t test and Wilcoxon rank sum test. $P<0.05$ was considered significant. 'n' represents the number of independent experiments.

Supplemental References

Burrell, A., Foy, C., and Burns, M. (2011). Applicability of three alternative instruments for food authenticity analysis: GMO identification. Biotechnology research international *2011*, 838232.

Eiraku, M., Watanabe, K., Matsuo-Takasaki, M., Kawada, M., Yonemura, S., Matsumura, M., Wataya, T., Nishiyama, A., Muguruma, K., and Sasai, Y. (2008). Self-organized formation of polarized cortical tissues from ESCs and its active manipulation by extrinsic signals. Cell stem cell *3*, 519-532.

Huang da, W., Sherman, B.T., and Lempicki, R.A. (2009). Systematic and integrative analysis of large gene lists using DAVID bioinformatics resources. Nat Protoc *4*, 44-57.

Kim, D., Pertea, G., Trapnell, C., Pimentel, H., Kelley, R., and Salzberg, S.L. (2013). TopHat2: accurate alignment of transcriptomes in the presence of insertions, deletions and gene fusions. Genome Biol *14*, R36.

Krueger, F., and Andrews, S.R. (2011). Bismark: a flexible aligner and methylation caller for Bisulfite-Seq applications. Bioinformatics *27*, 1571-1572.

Mitrpant, C., Porensky, P., Zhou, H., Price, L., Muntoni, F., Fletcher, S., Wilton, S.D., and Burghes, A.H. (2013). Improved antisense oligonucleotide design to suppress aberrant SMN2 gene transcript processing: towards a treatment for spinal muscular atrophy. PLoS One *8*, e62114.

Morizane, A., Doi, D., Kikuchi, T., Nishimura, K., and Takahashi, J. (2011). Small-molecule inhibitors of bone morphogenic protein and activin/nodal signals promote highly efficient neural induction from human pluripotent stem cells. J Neurosci Res *89*, 117-126.

Okita, K., Matsumura, Y., Sato, Y., Okada, A., Morizane, A., Okamoto, S., Hong, H., Nakagawa, M., Tanabe, K., Tezuka, K., *et al.* (2011). A more efficient method to generate integration-free human iPS cells. Nat Methods *8*, 409-412.

Ramskold, D., Wang, E.T., Burge, C.B., and Sandberg, R. (2009). An abundance of ubiquitously expressed genes revealed by tissue transcriptome sequence data. PLoS Comput Biol *5*, e1000598.

van der Steege, G., Grootscholten, P.M., van der Vlies, P., Draaijers, T.G., Osinga, J., Cobben, J.M., Scheffer, H., and Buys, C.H. (1995). PCR-based DNA test to confirm clinical diagnosis of autosomal recessive spinal muscular atrophy. Lancet *345*, 985-986.

Wada, T., Honda, M., Minami, I., Tooi, N., Amagai, Y., Nakatsuji, N., and Aiba, K. (2009). Highly efficient differentiation and enrichment of spinal motor neurons derived from human and monkey embryonic stem cells. PloS one *4*, e6722.

ARTHRITIS & RHEUMATOLOGY
Vol. 67, No. 1, January 2015, pp 302–314
DOI 10.1002/art.38912

Enhanced Chondrogenesis of Induced Pluripotent Stem Cells From Patients With Neonatal-Onset Multisystem Inflammatory Disease Occurs via the Caspase 1–Independent cAMP/Protein Kinase A/CREB Pathway

Koji Yokoyama,[1] Makoto Ikeya,[1] Katsutsugu Umeda,[1] Hirotsugu Oda,[2] Seishiro Nodomi,[1] Akira Nasu,[1] Yoshihisa Matsumoto,[3] Kazushi Izawa,[1] Kazuhiko Horigome,[4] Toshimasa Kusaka,[1] Takayuki Tanaka,[1] Megumu K. Saito,[1] Takahiro Yasumi,[1] Ryuta Nishikomori,[1] Osamu Ohara,[5] Naoki Nakayama,[6] Tatsutoshi Nakahata,[1] Toshio Heike,[1] and Junya Toguchida[1]

Objective. **Neonatal-onset multisystem inflammatory disease (NOMID) is a dominantly inherited autoinflammatory disease caused by NLRP3 mutations. NOMID pathophysiology is explained by the NLRP3 inflammasome, which produces interleukin-1β (IL-1β). However, epiphyseal overgrowth in NOMID is resistant to anti–IL-1 therapy and may therefore occur independently of the NLRP3 inflammasome. This study was undertaken to investigate the effect of mutated NLRP3 on chondrocytes using induced pluripotent stem cells (iPSCs) from patients with NOMID.**

Methods. **We established isogenic iPSCs with wild-type or mutant NLRP3 from 2 NOMID patients with NLRP3 somatic mosaicism. The iPSCs were differentiated into chondrocytes in vitro and in vivo. The phenotypes of chondrocytes with wild-type and mutant NLRP3 were compared, particularly the size of the chondrocyte tissue produced.**

Results. **Mutant iPSCs produced larger chondrocyte masses than wild-type iPSCs owing to glycosaminoglycan overproduction, which correlated with increased expression of the chondrocyte master regulator SOX9. In addition, in vivo transplantation of mutant cartilaginous pellets into immunodeficient mice caused disorganized endochondral ossification. Enhanced chondrogenesis was independent of caspase 1 and IL-1, and thus the NLRP3 inflammasome. Investigation of the human *SOX9* promoter in chondroprogenitor cells revealed that the CREB/ATF-binding site was critical for SOX9 overexpression caused by mutated NLRP3. This was supported by increased levels of cAMP and phosphorylated CREB in mutant chondroprogenitor cells.**

Conclusion. **Our findings indicate that the intrinsic hyperplastic capacity of NOMID chondrocytes is dependent on the cAMP/PKA/CREB pathway, independent of the NLRP3 inflammasome.**

Supported by Grants-in-Aid for Scientific Research from the Japanese Ministry of Health, Labor, and Welfare, the Japanese Ministry of Education, Culture, Sports, Science, and Technology (MEXT Leading Project for Realization of Regenerative Medicine), the Japanese Science and Technology Agency (Program for Intractable Diseases Research Utilizing Disease-Specific Induced Pluripotent Stem Cells), the Secom Science and Technology Foundation, and the Induced Pluripotent Stem Cell Research Fund.

[1]Koji Yokoyama, MD, Makoto Ikeya, PhD, Katsutsugu Umeda, MD, PhD, Seishiro Nodomi, MD, Akira Nasu, MD, PhD, Kazushi Izawa, MD, PhD, Toshimasa Kusaka, PhD, Takayuki Tanaka, MD, PhD, Megumu K. Saito, MD, PhD, Takahiro Yasumi, MD, PhD, Ryuta Nishikomori, MD, PhD, Tatsutoshi Nakahata, MD, PhD, Toshio Heike, MD, PhD, Junya Toguchida, MD, PhD: Kyoto University, Kyoto, Japan; [2]Hirotsugu Oda, MD: Kyoto University, Kyoto, Japan, and RIKEN Center for Integrative Medical Sciences, Yokohama, Japan; [3]Yoshihisa Matsumoto, MD, PhD: Kyoto University, Kyoto, Japan, and Nagoya City University, Nagoya, Japan; [4]Kazuhiko Horigome, PhD: Kyoto University, Kyoto, Japan, and Dainippon Sumitomo Pharma, Osaka, Japan; [5]Osamu Ohara, PhD: RIKEN Center for Integrative Medical Sciences, Yokohama, Japan, and Kazusa DNA Research Institute, Kisarazu, Japan; [6]Naoki Nakayama, PhD: University of Texas Health Science Center at Houston.

Address correspondence to Ryuta Nishikomori, MD, PhD, Department of Pediatrics, Kyoto University Graduate School of Medicine, 54 Kawahara-cho, Shogoin, Sakyo-ku, Kyoto 606-8507, Japan (e-mail: rnishiko@kuhp.kyoto-u.ac.jp); or to Junya Toguchida, MD, PhD, Department of Tissue Regeneration, Institute for Frontier Medical Sciences, Kyoto University, 53 Kawahara-cho, Shogoin, Sakyo-ku, Kyoto 606-8507, Japan (e-mail: togjun@frontier.kyoto-u.ac.jp).

Submitted for publication February 10, 2014; accepted in revised form October 7, 2014.

Systemic autoinflammatory syndromes are caused by defects in the innate immune system, especially pattern-recognition receptors, which result in uncontrolled inflammatory responses (1). Neonatal-onset multisystem inflammatory disease (NOMID) is a systemic autoinflammatory disease caused by NLRP3 mutation (2). The clinical features of NOMID include neonatal-onset persistent inflammation, urticarial rash, chronic aseptic meningitis, and arthropathy characterized by tumor-like expansive lesions in epiphyseal portions of long bones (3). NLRP3 is mainly expressed in hematopoietic cells, especially monocyte/macrophages, and in chondrocytes (4). In monocyte/macrophages, once NLRP3 is activated by its ligand, a multiprotein complex called the NLRP3 inflammasome forms, resulting in the activation of caspase 1, which cleaves pro–interleukin-1β (IL-1β) into active IL-1β (5–8).

The molecular mechanism by which NOMID-associated NLRP3 mutations lead to the activation of the NLRP3 inflammasome has not been fully elucidated. However, it is hypothesized that mutated NLRP3 can trigger the formation of the NLRP3 inflammasome independently of ligand binding, which causes dysregulated IL-1β secretion and uncontrolled multisystem inflammation. This hypothesis is supported by the fact that a targeted therapy against IL-1β effectively controls systemic inflammation in NOMID (9–11). However, epiphyseal overgrowth in NOMID is resistant to anti–IL-1 therapy (12).

Sequential radiologic imaging and histologic analyses of tissue biopsy specimens suggest that the main pathophysiology of NOMID arthropathy is not inflammation but disorganization of cartilage cell columns that leads to tumor-like expansive lesions (13). These clinical and pathologic findings suggest that mutant NLRP3 induces epiphyseal overgrowth in NOMID via mechanisms unrelated to the NLRP3 inflammasome. However, the function of NLRP3 in chondrocytes has not been elucidated, let alone the mechanism underlying epiphyseal overgrowth in NOMID.

Cartilage is a flexible connective tissue in the skeletal system and consists of chondrocytes and extracellular matrix (ECM). The growth plate consists of a column of chondrocytes that separate the epiphysis and metaphysis of a long bone. The primary function of these chondrocytes is to provide a cartilage template on which bone can form through endochondral ossification. In the growth plate, maturing chondrocytes are organized into resting, proliferating, prehypertrophic, and hypertrophic zones. Growth factor signaling stimulates mesenchymal progenitor cells in the resting zone to proliferate, upon which they move to the proliferating zone. These cells subsequently produce cartilage-specific ECM consisting of type II collagen and type XI collagens, and proteoglycans, such as aggrecan and cartilage oligomeric matrix protein. These cells then exit the cell cycle, differentiate, become hypertrophic, produce type X collagen and matrix metalloproteinases, and finally undergo apoptosis. The remaining cartilaginous matrix is mineralized and provides a scaffold on which bone can form (14,15).

It is difficult to obtain bone tissues from NOMID patients due to ethical reasons. Moreover, osteochondrogenic progenitor cells often cannot be obtained from postnatal human tissues in sufficient quantities, while acquiring such cells in sufficient quantities from human fetuses or embryos is ethically challenging. Furthermore, although a mass-like lesion called a "spike" is observed in mouse models of NOMID arthropathy (16), these models do not recapitulate the epiphyseal overgrowth observed in NOMID. These issues have prevented elucidation of the pathophysiologic mechanism underlying epiphyseal overgrowth in NOMID. In this study, we applied a newly developed chondrocyte differentiation system to induced pluripotent stem cells (iPSCs) derived from NOMID patients. This system allowed chondrocytes to be obtained in sufficient quantities to directly study the effect of mutated NLRP3 on chondrocyte phenotypes, focusing on the involvement of the NLRP3 inflammasome and the master regulator of chondrocyte differentiation, SOX9.

MATERIALS AND METHODS

Cell culture. Undifferentiated iPSCs from 2 NOMID patients with NLRP3 somatic mosaicism (p.Tyr570Cys and p.Gly307Ser) were established as previously described (17). From each patient, at least 3 clones of iPSCs with mutant or wild-type NLRP3 were established. In all experiments, mutant and wild-type isogenic cells were compared (3). Details of the procedure for culture of undifferentiated iPSCs and chondrogenic differentiation are available from the author upon request. The iPSCs were seeded onto a Matrigel (Becton Dickinson)–coated dish, cultured in mTeSR medium (StemCell Technologies) for 9 days, and then transferred to initial differentiation medium. This medium was changed once on day 3. On day 6, a single-cell suspension was prepared with 0.05% trypsin-EDTA. These cells were plated onto fibronectin-coated dishes, cultured in chondroprogenitor medium, and passaged every 3 days. We called these cells chondroprogenitor cells. For chondrogenesis, chondroprogenitor cells that had been passaged 3–5 times were used (Figure 1A).

Chondrogenesis assay. Serum-free chondrogenic medium has been described previously (18). Two-dimensional

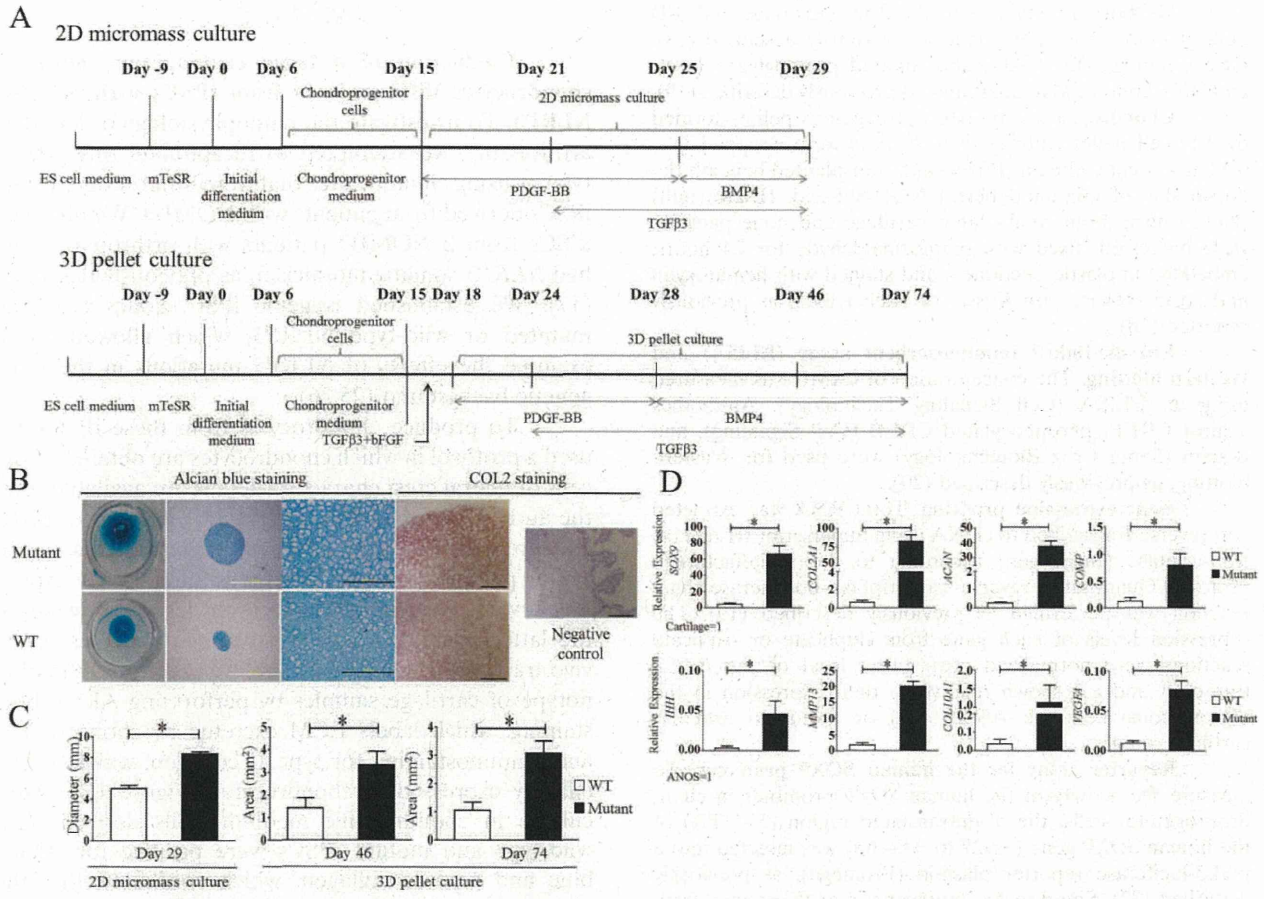

Figure 1. Successful differentiation of chondrocytes from induced pluripotent stem cells (iPSCs) with wild-type (WT) or mutant NLRP3 obtained from a patient with neonatal-onset multisystem inflammatory disease. **A,** Schematic representation of the culture conditions used to differentiate chondrocytes from iPSCs. **B,** Immunohistochemical staining of chondrocytes differentiated from iPSCs. Alcian blue staining of the 2-dimensional (2-D) micromass culture, Alcian blue staining of the 3-dimensional (3-D) pellet culture, higher-magnification images of Alcian blue staining of the 3-D pellet culture, anti–type II collagen (anti-COL2) antibody staining of the 3-D pellet culture, and anti–type II collagen antibody staining of mouse bladder (negative control) are shown. White bars = 2.0 mm; black bars = 0.2 mm. **C,** Quantitative analysis of the sizes of chondrocyte tissue masses in 2-D micromass cultures and 3-D pellet cultures. **D,** Cartilage-specific gene expression in 3-D pellet cultures. Expression of mRNA for each gene is shown relative to that in human cartilage (for *SOX9*, *COL2A1*, *ACAN*, and *COMP*) or the osteosarcoma cell line ANOS (for *IHH*, *MMP13*, *COL10A1*, and *VEGFA*), which were both set at 1. Bars in **C** and **D** show the mean ± SEM of 3 independent clones, from which duplicate measurements (**C**) or triplicate measurements (**D**) were obtained. Data are representative of 3 independent experiments and were obtained using iPSCs from patient 1 (p.Tyr570Cys); similar data were obtained using iPSCs from patient 2 (p.Gly307Ser). $* = P < 0.05$. ES = embryonic stem; PDGF-BB = platelet-derived growth factor BB; BMP-4 = bone morphogenetic protein 4; TGFβ3 = transforming growth factor β3; bFGF = basic fibroblast growth factor.

(2-D) micromass culture was performed by spotting a 5-μl droplet of chondroprogenitor cells (1.5×10^5) onto the well of a fibronectin-coated 24-well plate in serum-free chondrogenic medium supplemented with 40 ng/ml of platelet-derived growth factor BB (PDGF-BB; R&D Systems) and 1% fetal calf serum. The medium was changed every 3 days. Beginning on day 21, 10 ng/ml of transforming growth factor β3 (TGFβ3; R&D Systems) was added, and beginning on day 25, 40 ng/ml of PDGF-BB was replaced with 50 ng/ml of bone morphogenetic protein 4 (Wako). For 3-dimensional (3-D) pellet cultures, chondroprogenitor cells were passaged once in chondroprogenitor medium containing 5 ng/ml of basic fibroblast growth factor and 10 ng/ml of TGFβ3, and then cultured for 3 days. Aliquots of 2.5×10^5 cells were centrifuged to form pellets, which were cultured in 0.5 ml of serum-free chondrogenic medium supplemented with specific factors as outlined

above. Fixation and staining of the 2-D micromass and 3-D pellet cultures were performed as previously described (18). Glycosaminoglycan (GAG) and sulfated proteoglycan levels and DNA content were quantified as previously described (19).

Chondrogenesis in vivo. Cartilaginous pellets formed by 3-D cell pellet cultures over 20 days were wrapped in a 0.5 cm × 1 cm Gelfoam (Pfizer) and transplanted beneath the dorsal skin of immunodeficient NOD/Shi-scid, IL-2Rγ(null) (NOG) mice. Four weeks later, cartilage and bone particles were harvested, fixed with paraformaldehyde for 24 hours, embedded in plastic, sectioned, and stained with hematoxylin and eosin (H&E), von Kossa, or Alcian blue, as previously reported (18).

Enzyme-linked immunosorbent assay (ELISA) and Western blotting. The concentration of cAMP was measured using an ELISA (Cell Signaling Technology). Antibodies against CREB, phosphorylated CREB (Cell Signaling), and β-actin (Santa Cruz Biotechnology) were used for Western blotting, as previously described (20).

Gene expression profiling. Total RNA was extracted and reverse-transcribed to cDNA using Superscript III reverse transcriptase (Invitrogen) according to the manufacturer's protocol. Quantitative reverse transcriptase–polymerase chain reaction was performed as previously described (19). The expression levels of each gene from duplicate or triplicate reactions were normalized against the level of the *BACT* transcript and are shown relative to their expression in the osteosarcoma cell line ANOS (21) or a human articular cartilage sample.

Reporter assay for the human SOX9 promoter. To measure the activity of the human *SOX9* promoter in chondroprogenitor cells, the 5′-untranslated region (5′-UTR) of the human *SOX9* gene (−927 to +84 bp) was inserted into a pGL3-luciferase reporter plasmid (Promega), as previously described (22). Site-directed mutagenesis of the known transcription factor–binding sites of the human *SOX9* promoter was performed as previously described (23). The residue was mutated to the nucleotide that was least likely to be at this position, based on consensus sequences in the JASPAR transcription database (24). Sequence information is provided in Supplementary Figure 1, available on the *Arthritis & Rheumatology* web site at http://onlinelibrary.wiley.com/doi/10.1002/art.38912/abstract. Chondroprogenitor cells were plated at a density of 50,000 cells/well in 6-well plates, transfected with 2 μg of DNA/well using the FuGene 6 transfection reagent, and harvested 24 hours after transfection. Luciferase activity was measured as previously described (23). Additionally, 10 μ*M* forskolin (Sigma) and 10 μ*M* SQ22536 (Sigma) was used to activate and inhibit adenylate cyclase, respectively.

Ethics approval. This study was approved by the ethics committee of Kyoto University and was performed in accordance with the Declaration of Helsinki. A sample of human articular cartilage was obtained from a patient who underwent knee surgery and provided informed consent that the sample could be used for research purposes.

Statistical analysis. Data were analyzed using Student's *t*-test. *P* values less than 0.05 were considered significant.

RESULTS

Production of a large cartilaginous mass by chondrocytes differentiated from iPSCs with mutated NLRP3. To investigate the pathophysiology of NOMID arthropathy, we attempted to recapitulate this phenotype by using chondrocytes that were differentiated from iPSCs derived from patients with NOMID. We obtained iPSCs from 2 NOMID patients with arthropathy who had *NLRP3* somatic mosaicism, as previously described (17). We established isogenic iPSC clones that had mutated or wild-type NLRP3, which allowed us to examine the effects of NLRP3 mutations in the same genetic background (25,26).

To produce chondrocytes from these iPSCs, we used a protocol in which chondrocytes are obtained from cells of neural crest character (details are available from the author upon request) (Figure 1A). We performed 2 chondrogenic assays, a 2-D micromass culture assay and a 3-D pellet assay. The former is suitable for experiments with exogenous inhibitors or activators, whereas the latter generates more mature chondrocytes for in vivo transplantation assay. First, we confirmed the phenotype of cartilage samples by performing Alcian blue staining, which labels ECM excreted by chondrocytes, and immunostaining for type II collagen, which is specifically expressed in chondrocytes (Figure 1B). After culture in chondrogenic medium, cells derived from wild-type and mutant iPSCs were positive for Alcian blue and type II collagen, which confirmed that the iPSCs had successfully differentiated into chondrocytes. Importantly, the 2-D micromass and 3-D pellet samples derived from mutant iPSCs were significantly larger than those derived from wild-type iPSCs, up to day 74 of culture (Figures 1B and C).

Next, we examined the expression of mRNA for cartilage-related genes expressed in proliferating chondrocytes (early markers; *SOX9*, *COL2A1*, *ACAN*, and *COMP*) and those expressed in hypertrophic chondrocytes (late markers; *IHH*, *MMP13*, *COL10A1*, and *VEGFA*) in samples obtained by the method described above (Figure 1D). These genes were expressed in 3-D pellet samples obtained from mutant and wild-type iPSCs, further indicating that chondrocyte differentiation was successful and that 3-D pellets contained chondrocytes at various differentiation stages. The expression levels of both early and late chondrogenic markers were significantly higher in mutant samples than in wild-type samples (Figure 1D). Taken together, these data show that chondrocytes were successfully differentiated in

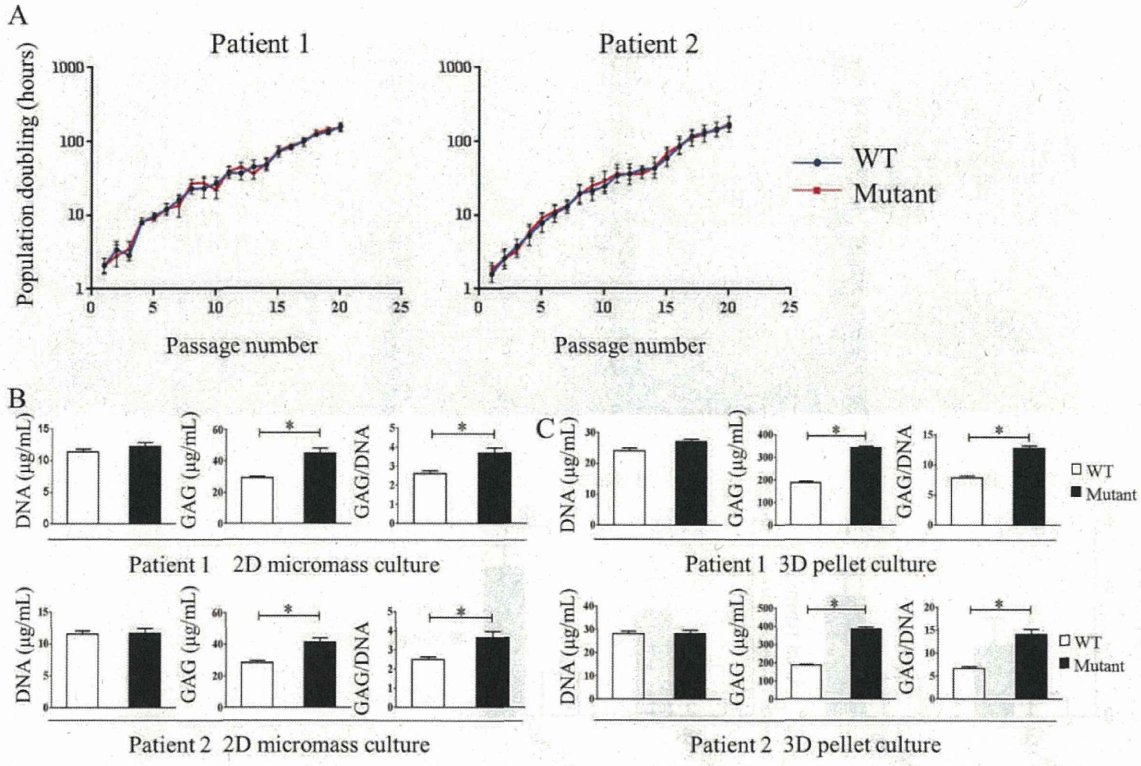

Figure 2. Formation of large cartilaginous masses by mutant iPSCs from patients with neonatal-onset multisystem inflammatory disease is due to the overproduction of extracellular matrix and not due to increased cell proliferation. **A,** Growth curves of chondroprogenitor cells differentiated from mutant and wild-type iPSCs. Values are the mean ± SEM of 3 independent clones, from which duplicate measurements were obtained. **B** and **C,** DNA concentration, glycosaminoglycan (GAG) concentration, and the ratio of GAG concentration to DNA concentration in 2-D micromass (**B**) and 3-D pellet (**C**) cultures. Bars show the mean ± SEM of 3 independent clones, from which triplicate (**B**) or duplicate (**C**) measurements were obtained. Data are representative of 3 independent experiments with consistent results. * = $P < 0.05$. See Figure 1 for other definitions.

vitro from iPSCs derived from NOMID patients, and that chondrocytes differentiated from iPSCs with mutant *NLRP3* produce large cartilaginous masses in vitro. They also demonstrate that the entire chondrocyte differentiation process, from precursors to late chondrocytes, is enhanced in mutant cells compared to wild-type cells.

The production of large cartilaginous masses by mutant iPSCs is due to ECM overproduction, not to increased cell proliferation. We next sought to determine what causes the chondrocyte masses derived from mutant iPSCs to be larger than those derived from wild-type iPSCs. First, we analyzed the proliferation potential of chondroprogenitor cells. Population doubling time did not significantly differ between mutant and wild-type chondroprogenitor cells up to 15 passages, after which the cells stopped proliferating (Figure 2A). Next, we determined the number of differentiated chondrocytes by analyzing DNA content and GAG production, which is a major cartilaginous ECM component. In 2-D micromass and 3-D pellet cultures, the DNA content in differentiated chondrocyte tissue derived from mutant and wild-type iPSCs did not significantly differ. This suggests that a similar number of chondrocytes were produced from mutant and wild-type iPSCs. In contrast, chondrocytes derived from mutant iPSCs produced more GAG than those derived from wild-type iPSCs in 2-D micromass culture (Figure 2B) and 3-D pellet culture (Figure 2C). These data indicate that the larger amount of chondrocyte tissue produced from mutant iPSCs is not due to an increased number of chondrocytes, but to an increased amount of cartilaginous ECM produced per cell.

In vivo differentiation of chondrocytes from mutant iPSCs reveals dysregulated endochondral ossification. Radiologic examination of affected long bones in NOMID patients shows enlargement of the epiphysis

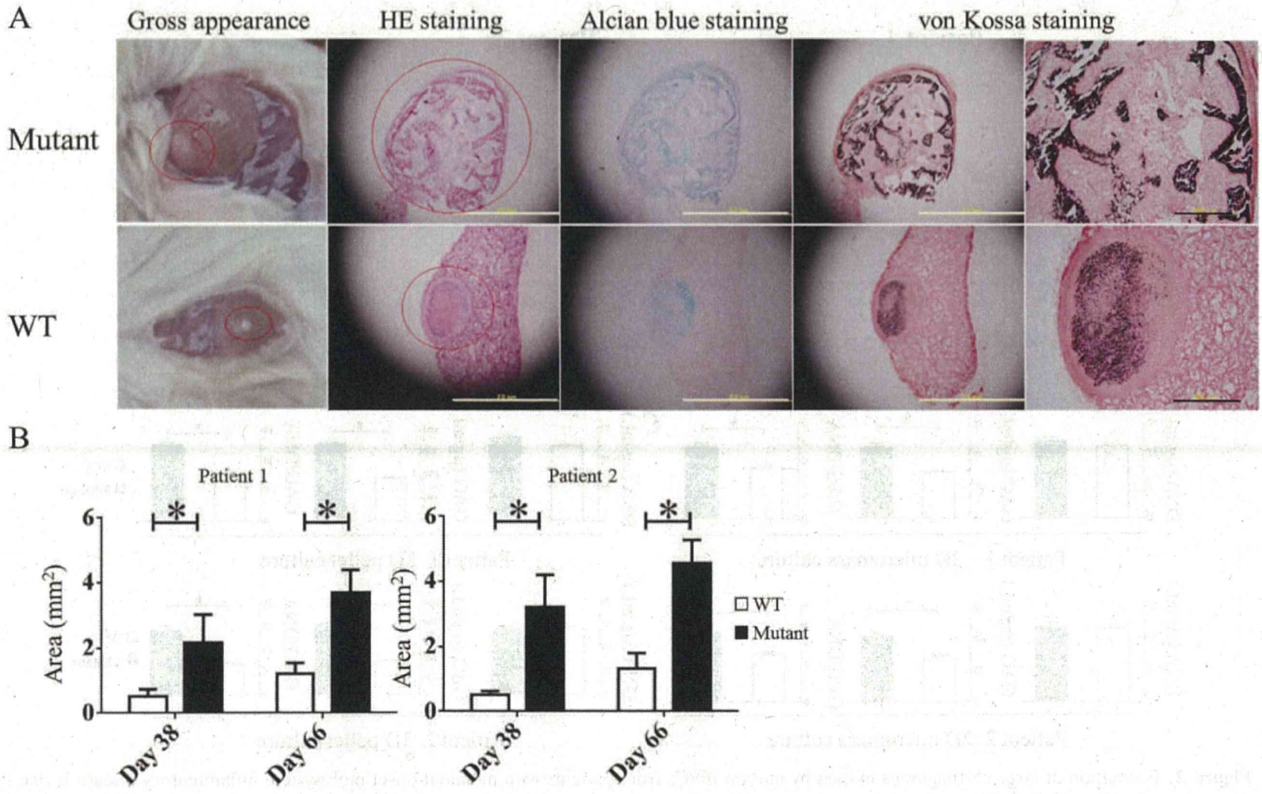

Figure 3. In vivo maturation of 3-D cell pellets derived from mutant or wild-type iPSCs from patients with neonatal-onset multisystem inflammatory disease. **A,** Images of 3-D cell pellets derived from mutant or wild-type iPSCs following transplantation into immunodeficient mice. Gross appearance, hematoxylin and eosin (H&E) staining, Alcian blue staining, von Kossa staining, and higher-magnification images of von Kossa staining are shown. Red circles indicate bone or cartilage pellets in gel form. White bars = 2.0 mm; black bars = 0.2 mm. Results shown were obtained using iPSCs from patient 1; similar results were obtained using iPSCs from patient 2. **B,** Quantitative analysis of the size of pellets when they were transplanted (day 38) and harvested (day 66). Bars show the mean ± SEM of 3 independent clones, from which duplicate measurements were obtained. Data are representative of 3 independent experiments. * = $P < 0.05$. See Figure 1 for other definitions.

with abnormal ossification. The in vitro differentiation system did not induce chondrocyte calcification, probably due to the lack of cell components or factors necessary for the final differentiation step. Therefore, we used an in vivo differentiation system as a model for endochondral ossification, in which immature 3-D pellet samples were transplanted into NOG mice. The transplanted cartilage mass was vascularized in vivo (Figure 3A). Mutant pellets were larger than wild-type pellets, both at transplantation and harvesting, and this size difference increased during in vivo differentiation (Figure 3B). Following von Kossa staining, which detects calcium deposits, calcification was detected in both wild-type and mutant pellets (Figure 3A). Interestingly, Alcian blue staining revealed that mutant pellets contained more residual cartilage components than wild-type pellets. In addition, calcified areas were scattered throughout mutant pellets, whereas they were localized in specific regions and were clearly separated from Alcian blue–positive areas in wild-type pellets. Taken together, these data indicate that in our in vivo model, chondrocyte tissue differentiated from mutant iPSCs grows larger and exhibits disorganized ossification compared to chondrocyte tissue differentiated from wild-type iPSCs.

The enhanced chondrogenesis of mutant iPSCs is independent of the NLRP3 inflammasome. The inflammatory phenotype of NOMID is caused by gain-of-function NLRP3 mutations, leading to activation of the NLRP3 inflammasome (27). Therefore, we examined the involvement of the NLRP3 inflammasome in the formation of cartilaginous masses. First, we analyzed the

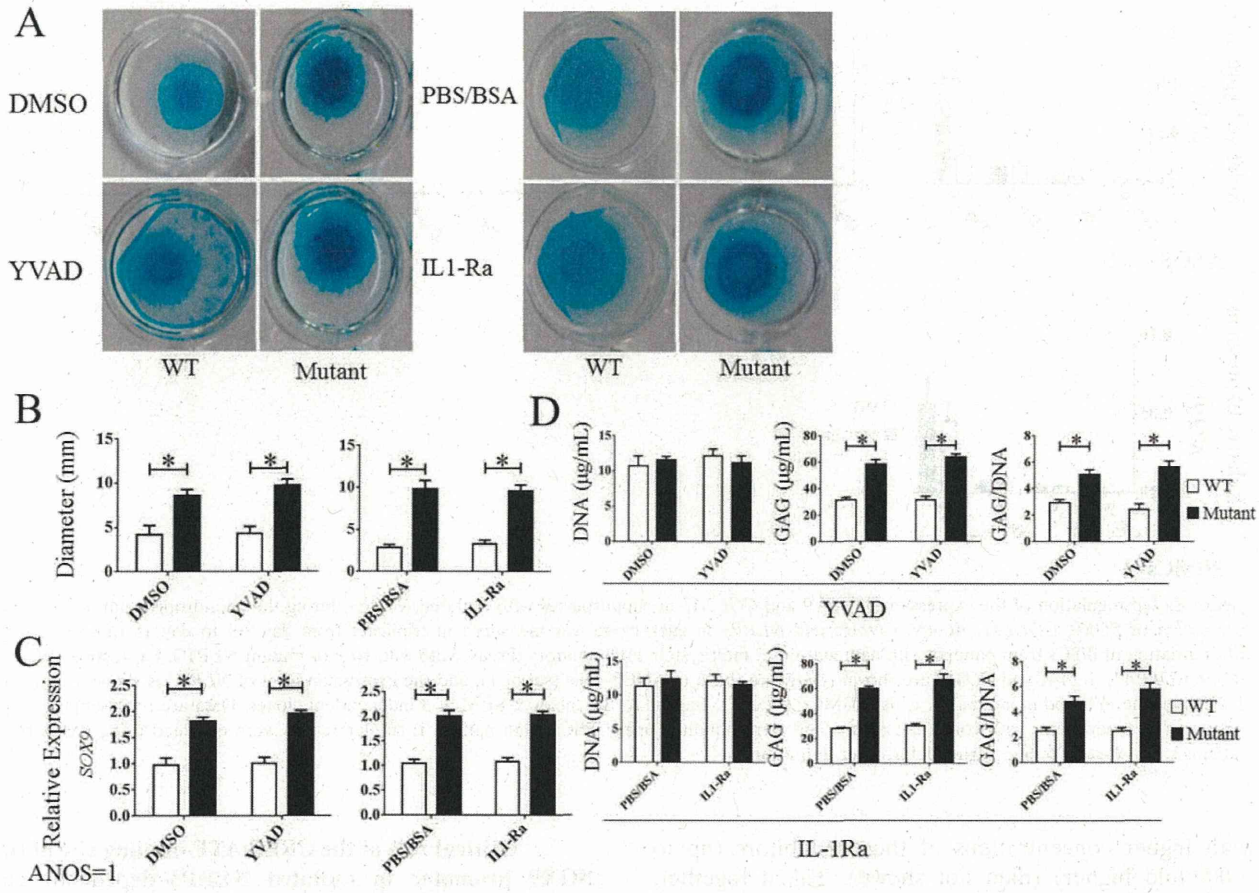

Figure 4. NLRP3 inflammasome–independent enhanced chondrogenesis of mutant iPSCs from patients with neonatal-onset multisystem inflammatory disease. Wild-type and mutant iPSCs were differentiated into chondrocytes in 2-D micromass cultures, and the caspase 1 inhibitor Ac-YVAD-CHO (YVAD; 10 μM) or human recombinant interleukin-1 receptor antagonist (IL-1Ra; 1 μg/ml) was added to the cultures. Control cultures were incubated with DMSO or phosphate buffered saline (PBS) containing bovine serum albumin (BSA). **A**, Representative 2-D micromass cultures treated with YVAD or DMSO as control (left) or with IL-1Ra or PBS/BSA as control (right). **B**, Diameter of the micromass. **C**, *SOX9* expression in chondrocytes derived from wild-type and mutant iPSCs and treated with YVAD or IL-1Ra. Expression levels are shown relative to those in ANOS cells (set at 1). **D**, DNA concentration, glycosaminoglycan (GAG) concentration, and the ratio of GAG concentration to DNA concentration in chondrocytes derived from wild-type or mutant iPSCs and treated with YVAD or IL-1Ra. Bars show the mean ± SEM of 3 independent clones from which triplicate measurements were obtained. Data are representative of 3 independent experiments. Data shown were obtained using iPSCs from patient 1; similar results were obtained using iPSCs from patient 2. $* = P < 0.05$. See Figure 1 for other definitions.

expression of the NLRP3 inflammasome components in 2-D cartilage samples. Mutant and wild-type cartilage samples both expressed NLRP3, but did not express ASC, pro–caspase 1, or pro–IL-1β by Western blotting (data not shown). This suggests that the formation of large cartilaginous masses by mutant chondrocytes occurs independently of the NLRP3 inflammasome.

To confirm that chondrogenesis of mutant iPSCs is enhanced independently of the NLRP3 inflammasome, we used inhibitors of components of the NLRP3 inflammasome, namely, Ac-YVAD-CHO, which inhibits caspase 1, and recombinant human IL-1 receptor antagonist (IL-1Ra), which antagonizes IL-1. Neither Ac-YVAD-CHO (10 μM) treatment nor recombinant human IL-1Ra (1 μg/ml) treatment during 2-D micromass culture prevented the formation of large cartilaginous masses (Figures 4A and B), *SOX9* upregulation (Figure 4C), or overproduction of GAG (Figure 4D) by chondrocytes derived from mutant iPSCs. The same was true when samples were treated

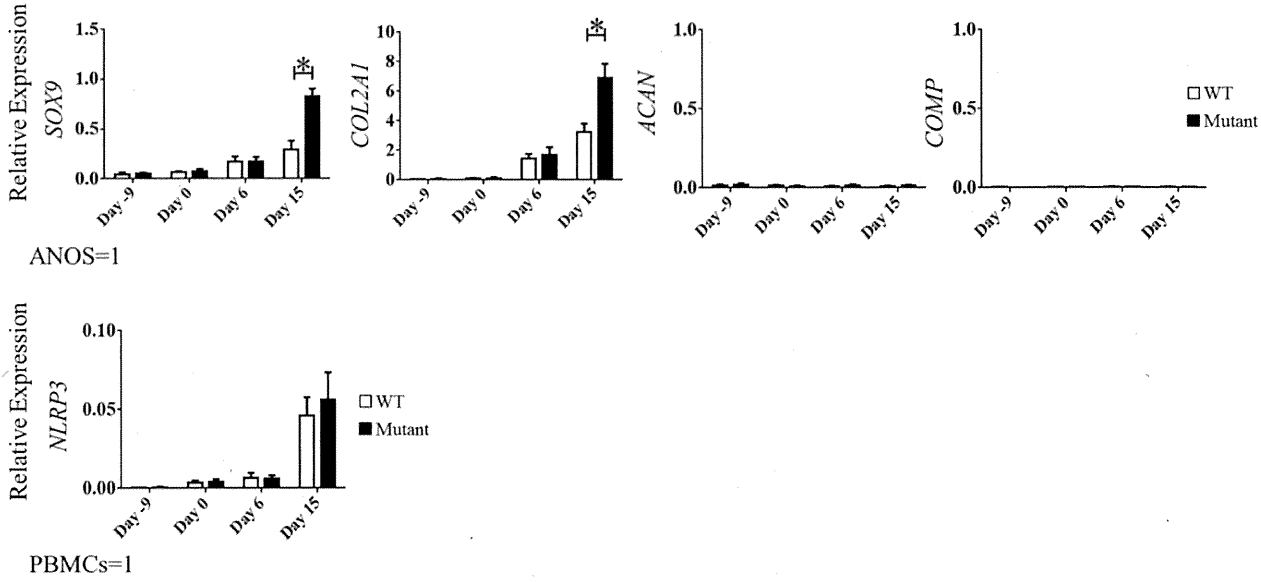

Figure 5. Up-regulation of the expression of *SOX9* and *COL2A1* in chondrocytes with mutated *NLRP3* during the chondroprogenitor cell stage. Expression of *SOX9*, *COL2A1*, *ACAN*, *COMP*, and *NLRP3* in each clone was measured in triplicate from day −9 to day 15 of chondrocyte differentiation of iPSCs from patients with neonatal-onset multisystem inflammatory disease with wild-type or mutant NLRP3. Expression levels of *SOX9*, *COL2A1*, *ACAN*, and *COMP* are shown relative to those in ANOS cells (set at 1), and the expression level of *NLRP3* is shown relative to that in peripheral blood mononuclear cells (PBMCs; set at 1). Bars show the mean ± SEM of 3 independent clones. Data are representative of 3 independent experiments with consistent results and were obtained using iPSCs from patient 1; similar results were obtained using iPSCs from patient 2. * = $P < 0.05$. See Figure 1 for other definitions.

with higher concentrations of these inhibitors (up to 1,000-fold higher) (data not shown). Taken together, these data strongly indicate that the enhanced chondrogenesis of mutant iPSCs is independent of caspase 1 and IL-1, and thus the NLRP3 inflammasome.

Correlation of the up-regulation of NLRP3 with the up-regulation of SOX9 in chondroprogenitor cells. To dissect the mechanism underlying the enhanced chondrogenesis of mutant iPSCs, we analyzed the time course of chondrocyte-specific gene expression in chondroprogenitor cells (Figure 5). Expression of *SOX9*, *COL2A1*, and *NLRP3* started to be up-regulated in chondroprogenitor cells on day 6. Importantly, on day 15, *SOX9* and *COL2A1* were up-regulated more in mutant chondroprogenitor cells than in wild-type chondroprogenitor cells, whereas *NLRP3* was up-regulated similarly in both types of cells (Figure 5). In contrast, at this time point, the other chondrocyte-specific markers *ACAN* and *COMP* were not expressed in either type of cell (Figure 5). Thus, differential up-regulation of *SOX9* in chondroprogenitor cells correlated with the up-regulation of *NLRP3* and preceded the up-regulation of *COMP* and *ACAN*.

Critical role of the CREB/ATF-binding site of the SOX9 promoter in mutated NLRP3–dependent enhancement of SOX9 expression. Next, we focused on *SOX9* because it was up-regulated together with *NLRP3*, and this preceded the up-regulation of other chondrocyte-specific markers. We analyzed the activity of the human *SOX9* promoter in chondroprogenitor cells in which the level of *SOX9* mRNA was increased. We created a luciferase reporter construct containing the 5′-UTR of human *SOX9*, which encompasses −927 to +84 bp of the transcription start site. This fragment has basal promoter activity and putative binding sites for 5 transcription factors, namely, NF-AT, activator protein 1 (AP-1), NF-κB, Sp1, and CREB/ATF (see Supplementary Figure 1, available on the *Arthritis & Rheumatology* web site at http://onlinelibrary.wiley.com/doi/10.1002/art.38912/abstract). This fragment showed no promoter activity in the monocytic cell line THP-1 or the erythroleukemic cell line K562, which do not express endogenous *SOX9* (data not shown). Importantly, human *SOX9* promoter activity was higher in mutant chondroprogenitor cells than in wild-type chondroprogenitor cells (Figure 6A). To identify the element of the human *SOX9*

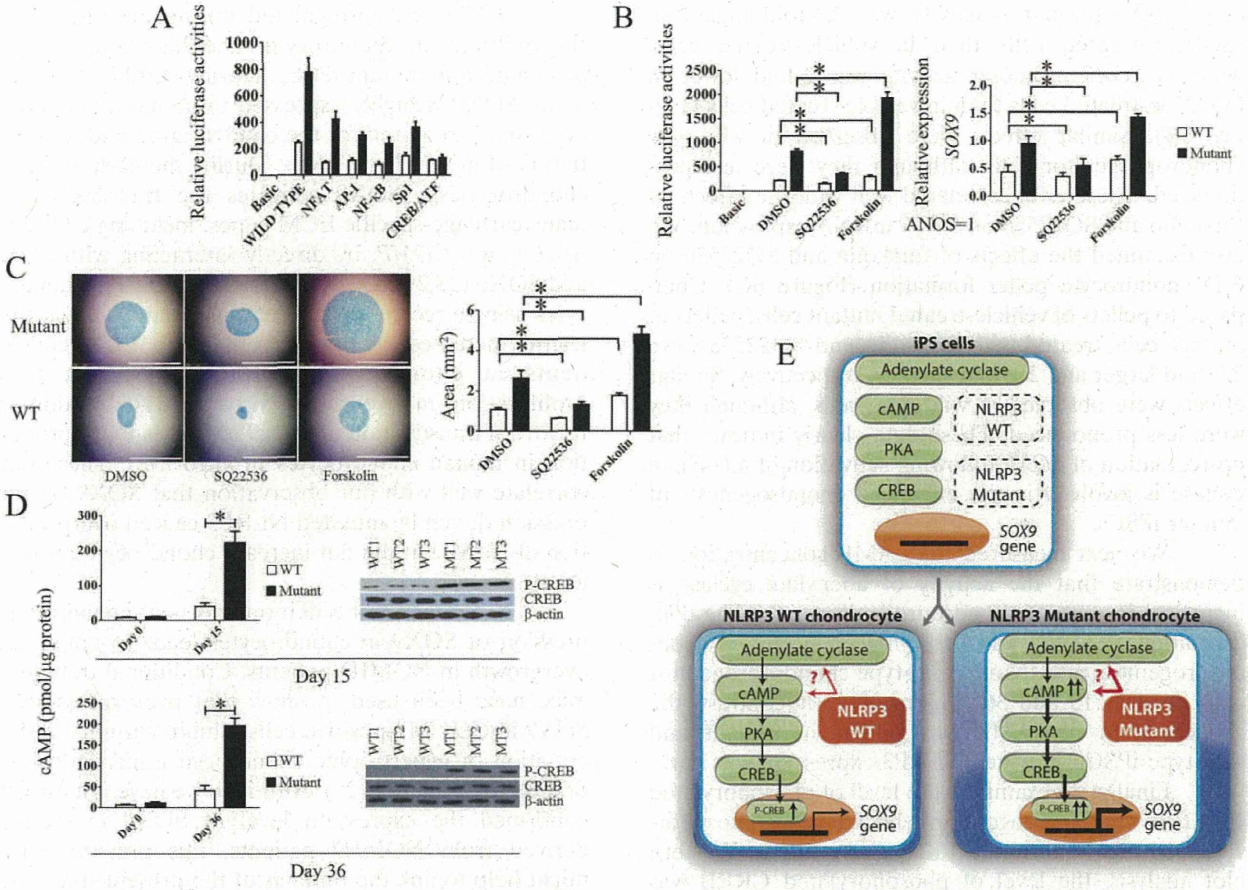

Figure 6. *SOX9* up-regulation in chondrocytes derived from iPSCs from patients with neonatal-onset multisystem inflammatory disease with mutant NLRP3 is dependent on the cAMP/protein kinase A (PKA)/CREB pathway. **A,** *SOX9* promoter activity in wild-type and mutant chondroprogenitor cells after the introduction of mutations into its transcription factor binding sites. **B,** *SOX9* promoter activity and expression in wild-type and mutant chondroprogenitor cells treated with SQ22536 or forskolin. **C,** Effects of SQ22536 and forskolin on 3-D pellets of mutant and wild-type cells. Both reagents were used at a concentration of 10 μM. Bars = 2.0 mm. **D,** Increased activity of the cAMP/PKA/CREB pathway in mutant chondroprogenitor cells compared to wild-type chondroprogenitor cells, as demonstrated by cAMP concentration in wild-type and mutant iPSCs (day 0) and chondroprogenitor cells (day 15 and day 36), and Western blot analysis of phosphorylated CREB in wild-type (WT1–3) and mutant (MT1–3) chondroprogenitor cells. **E,** Schematic diagram summarizing the molecular mechanism elucidated in this study. Bars in **A–D** show the mean ± SEM of 3 independent clones from which triplicate (**A, B,** and **D**) or duplicate (**C**) measurements were obtained. Data are representative of 2 independent experiments with consistent results and were obtained using iPSCs from patient 1; similar results were obtained using iPSCs from patient 2. $* = P < 0.05$. See Figure 1 for other definitions.

promoter region that responds in a mutated NLRP3–dependent manner, we performed site-directed mutagenesis of the sites of this promoter that bind the transcription factors NF-AT, AP-1, NF-κB, Sp1, and CREB/ATF (Supplementary Figure 1). Among the reporters with these mutations, the reporter that harbored a mutation in the CREB/ATF-binding site showed the least up-regulation of *SOX9* promoter activity in mutant cells (Figure 6A and Supplementary Figure 1). Thus, we speculate that the CREB/ATF-binding site is critical for activation of the human *SOX9* promoter in a mutated NLRP3–dependent manner.

Critical role of the cAMP/PKA/CREB pathway in SOX9 up-regulation caused by mutated NLRP3. To further explore the association between mutated NLRP3 and the cAMP/PKA/CREB pathway, we examined the effect of an adenylate cyclase activator and inhibitor (forskolin and SQ22536, respectively) on the activity of the human *SOX9* promoter and *SOX9* mRNA expression (Figure 6B). Among mutant chondroprogenitor

cells, *SOX9* promoter activity was 2.3-fold higher in forskolin-treated cells than in vehicle-treated cells, whereas *SOX9* promoter activity was 2-fold lower in SQ22536-treated cells than in vehicle-treated cells (Figure 6B). Similar effects were observed in wild-type chondroprogenitor cells, although they were less pronounced. These data correlated well with the effects of forskolin and SQ22536 on *SOX9* mRNA expression. We also examined the effects of forskolin and SQ22536 on 3-D chondrocyte pellet formation (Figure 6C). Compared to pellets of vehicle-treated mutant cells, pellets of mutant cells treated with forskolin and SQ22536 were 2.0-fold larger and 2.1-fold smaller, respectively. Similar effects were observed in wild-type cells, although they were less pronounced. These data clearly indicate that up-regulation of *SOX9* following activation of adenylate cyclase is involved in the enhanced chondrogenesis of mutant iPSCs.

We next measured the cAMP concentration to demonstrate that the activity of adenylate cyclase is increased in mutant chondroprogenitor cells. The concentration of cAMP was 4-fold higher in mutant chondroprogenitor cells than in wild-type chondroprogenitor cells on days 15 and 36 (Figure 6D). By contrast, the concentration of cAMP was similar in mutant and wild-type iPSCs, in which NLRP3 expression was low.

Finally, we examined the level of phosphorylated CREB in chondroprogenitor cells. CREB is phosphorylated by cAMP-activated PKA. According to Western blot analysis, the level of phosphorylated CREB was higher in mutant chondroprogenitor cells than in wild-type chondroprogenitor cells on days 15 and 36 (Figure 6D). Taken together, these data indicate that the cAMP/PKA/CREB pathway plays an important role in the up-regulation of *SOX9*, and therefore enhanced chondrogenesis, in chondroprogenitor cells with mutant NLRP3 (Figure 6E).

DISCUSSION

Disease-specific iPSCs have been used extensively to investigate the pathogenesis of diseases and to discover novel drugs. This approach is particularly useful to study rare diseases because tissues are often difficult to obtain from patients with such diseases. In this study, we used disease-specific iPSCs to study NOMID. Using this approach, we produced chondrocyte tissues with mutant and wild-type NLRP3, and revealed a previously unidentified connection between the inflammasome-associated molecule NLRP3 and the master regulator of chondrocyte differentiation SOX9.

SOX9 was up-regulated during the differentiation of iPSCs into chondrocytes, and this was particularly pronounced in mutant iPSCs. During cartilage development, SOX9 is highly expressed in immature chondrocytes and is required for the condensation and differentiation of mesenchymal cells. During the early stages of chondrogenesis, SOX9 activates the transcription of many cartilage-specific ECM genes, including *COL2A1*, *ACAN*, and *COMP*, by directly interacting with SOX5 and SOX6 (28,29). Overexpression of *SOX9* in chondrocytes using a recombinant adeno-associated virus significantly increases the synthesis of major ECM components in chondrocytes, without affecting their proliferation, in vivo and in vitro (30,31). In addition, retroviral transduction of SOX9 increases ECM production in human chondrocytes in vitro (32). These data correlate well with our observation that SOX9 overexpression driven by mutated NLRP3 caused overproduction of ECM, but did not increase chondrocyte proliferation.

It remains to be determined how enhanced expression of SOX9 in chondrocytes leads to epiphyseal overgrowth in NOMID patients. Conditional transgenic mice have been used to show that overexpression of *SOX9* in *COL2A1*-positive cells inhibits terminal differentiation of hypertrophic chondrocytes and endochondral bone formation (29). Although we have not directly confirmed the expression level of SOX9 in samples derived from NOMID patients, this previous study might help to link the findings of the present study with the clinical phenotype of NOMID patients.

We identified the cAMP/PKA/CREB pathway as being critical for the up-regulation of *SOX9* mRNA in a mutant NLRP3–dependent manner. cAMP is an intracellular second messenger that is involved in a variety of cellular processes (33). cAMP/PKA/CREB signaling is crucial in chondrogenesis, and synergism between cAMP and SOX9 is particularly important (34–36). Cotransfection of CREB binding protein (CBP) and p300 increases SOX9 activity (35). PKA phosphorylates SOX9 and thereby increases SOX9 activity, which results in the up-regulation of the *COL2A1* promoter through the interaction between CBP and SOX9 (34). In addition, the PKA inhibitor H89 blocks chondrogenesis in the chick limb bud (36). These data support the idea that cAMP/PKA/CREB signaling up-regulates SOX9 to enhance chondrogenesis.

Using stromal cells established from a tumor-like lesion in a NOMID patient, Almeida et al (37) demonstrated that activation of the cAMP/PKA/CREB pathway leads to caspase 1 activation, release of IL-1β, and

consequently the proliferation of bone stromal cells. This suggests that bone lesions in NOMID are caused in an NLRP3 inflammasome–dependent manner. One explanation for the discrepancy between their data and ours is that no disease-causing NLRP3 mutation was identified in the patient in that previous study; therefore, an unknown genetic alteration may have caused the NOMID phenotype. Another explanation is that different cell types were analyzed in the two studies. The previous study analyzed bone stromal cells established from a tumor-like lesion that might have been a heterogeneous population, while we focused on a single cell type, namely, chondrocytes.

The lack of environmental factors and interactions with other cell populations in our model might have eliminated some contributions of the NLRP3 inflammasome and IL-1β pathway that occur in NOMID patients. Furthermore, our observations relied on an artificial differentiation system in which iPSCs were first differentiated into cells of neural crest character and then into chondrocytes by culture in the presence of various exogenous factors. Abnormal epiphyseal growth is specifically observed around the knee joints of NOMID patients; therefore, additional events might be required to trigger abnormal chondrocyte proliferation in vivo. It is also possible that specific factors produced by surrounding cells in unaffected joints prevent mutant chondrocytes from manifesting their phenotype. Further analyses of patients or patient-derived samples would provide a better understanding of the pathophysiology of arthropathy in NOMID.

The interaction between cAMP and NLRP3 has been studied in monocyte/macrophages, in which the NLRP3 inflammasome is activated following binding of extracellular Ca^{2+} to Ca^{2+}-sensing receptors (CaSRs) (38,39). One study reported that an increase in extracellular Ca^{2+} is detected by CaSRs, which leads to phospholipase C activation and subsequently the release of Ca^{2+} from the endoplasmic reticulum and down-regulation of cAMP. cAMP binds directly to NLRP3 and inhibits assembly of the NLRP3 inflammasome. Therefore, this decrease in the level of intracellular cAMP relieves this inhibition and thereby induces activation of the NLRP3 inflammasome (38). On the other hand, another study reported that an increase in the extracellular Ca^{2+} concentration induces an increase in the intracellular Ca^{2+} concentration, thereby leading to activation of the NLRP3 inflammasome, and this mechanism requires the CaSRs GPRC6A and CaSR, but not the down-regulation of cAMP (39). Thus, the effects of cAMP on the NLRP3 inflammasome in monocyte/macrophages remain a subject of controversy.

In the chondrocyte differentiation system used in the present study, mutated NLRP3 caused SOX9 overexpression via the cAMP/PKA/CREB pathway, which is at odds with the relationship between cAMP and activation of the NLRP3 inflammasome in monocyte/macrophages. This discrepancy might be explained by the absence of other NLRP3 inflammasome components, such as ASC and procaspase 1, in the chondrocytes generated in the present study. Further analysis is needed to determine why cAMP/PKA/CREB signaling elicits different effects on mutated NLRP3 in chondrocytes and monocyte/macrophages, as well as how intracellular cAMP is up-regulated in chondrocytes derived from mutant iPSCs.

There have been many reports on the differentiation of chondrocytes from embryonic stem cells (ESCs) or iPSCs (40–42). However, previously, it was difficult to differentiate a sufficient number of chondrocytes with a relatively mature phenotype from ESCs or iPSCs, especially human ESCs or iPSCs. We have recently established a cartilage differentiation system in which iPSCs first differentiate into cells of neural crest character and then into chondrocytes, which enabled us to obtain a large number of chondrocytes with the phenotype of growth plate cartilage chondrocytes. An important aspect of the present study is that this differentiation system can generate a large number of chondrocytes that could share functional properties causing the arthropathy observed in NOMID. This system could thereby be used to screen for novel therapeutic agents.

In conclusion, we showed that SOX9 is overexpressed via the cAMP/PKA/CREB signaling pathway in chondrocytes with disease-causing mutations in NLRP3, and this causes overproduction of ECM independently of the NLRP3 inflammasome. We used iPSC technology to elucidate the role of chondrocytes in the pathophysiology of the human disease NOMID.

ACKNOWLEDGMENTS

We are grateful to K. Hayakawa, M. Fukuta, S. Nagata, and M. Hiraga of Kyoto University for technical assistance and to N. Kambe of Chiba University for critical reading of the manuscript.

AUTHOR CONTRIBUTIONS

All authors were involved in drafting the article or revising it critically for important intellectual content, and all authors approved the final version to be published. Drs. Nishikomori and Toguchida had

full access to all of the data in the study and take responsibility for the integrity of the data and the accuracy of the data analysis.
Study conception and design. Yokoyama, Ikeya, Tanaka, Nishikomori, Nakayama, Nakahata, Heike, Toguchida.
Acquisition of data. Yokoyama, Umeda, Nodomi, Horigome, Kusaka, Ohara.
Analysis and interpretation of data. Yokoyama, Umeda, Oda, Nodomi, Nasu, Matsumoto, Izawa, Kusaka, Saito, Yasumi, Nishikomori, Ohara.

ADDITIONAL DISCLOSURES

Author Horigome is an employee of Dainippon Sumitomo Pharma.

REFERENCES

1. Kufer TA, Sansonetti PJ. NLR functions beyond pathogen recognition. Nat Immunol 2011;12:121–8.
2. Hoffman HM, Mueller JL, Broide DH, Wanderer AA, Kolodner RD. Mutation of a new gene encoding a putative pyrin-like protein causes familial cold autoinflammatory syndrome and Muckle-Wells syndrome. Nat Genet 2001;29:301–5.
3. Tanaka N, Izawa K, Saito MK, Sakuma M, Oshima K, Ohara O, et al. High incidence of NLRP3 somatic mosaicism in patients with chronic infantile neurologic, cutaneous, articular syndrome: results of an international multicenter collaborative study. Arthritis Rheum 2011;63:3625–32.
4. Feldmann J, Prieur AM, Quartier P, Berquin P, Certain S, Cortis E, et al. Chronic infantile neurological cutaneous and articular syndrome is caused by mutations in CIAS1, a gene highly expressed in polymorphonuclear cells and chondrocytes. Am J Hum Genet 2002;71:198–203.
5. Latz E, Xiao TS, Stutz A. Activation and regulation of the inflammasomes. Nat Rev Immunol 2013;13:397–411.
6. Gattorno M, Martini A. Beyond the NLRP3 inflammasome: autoinflammatory diseases reach adolescence [review]. Arthritis Rheum 2013;65:1137–47.
7. Bauernfeind FG, Horvath G, Stutz A, Alnemri ES, MacDonald K, Speert D, et al. NF-κB activating pattern recognition and cytokine receptors license NLRP3 inflammasome activation by regulating NLRP3 expression. J Immunol 2009;183:787–91.
8. Mariathasan S, Weiss DS, Newton K, McBride J, O'Rourke K, Roose-Girma M, et al. Cryopyrin activates the inflammasome in response to toxins and ATP. Nature 2006;440:228–32.
9. Hoffman HM, Rosengren S, Boyle DL, Cho JY, Nayar J, Mueller JL, et al. Prevention of cold-associated acute inflammation in familial cold autoinflammatory syndrome by interleukin-1 receptor antagonist. Lancet 2004;364:1779–85.
10. Hawkins PN, Lachmann HJ, McDermott MF. Interleukin-1-receptor antagonist in the Muckle-Wells syndrome. N Engl J Med 2003;348:2583–4.
11. Lachmann HJ, Kone-Paut I, Kuemmerle-Deschner JB, Leslie KS, Hachulla E, Quartier P, et al. Use of canakinumab in the cryopyrin-associated periodic syndrome. N Engl J Med 2009;360:2416–25.
12. Arostegui JI, Lopez Saldana MD, Pascal M, Clemente D, Aymerich M, Balaguer F, et al. A somatic NLRP3 mutation as a cause of a sporadic case of chronic infantile neurologic, cutaneous, articular syndrome/neonatal-onset multisystem inflammatory disease: novel evidence of the role of low-level mosaicism as the pathophysiologic mechanism underlying Mendelian inherited diseases. Arthritis Rheum 2010;62:1158–66.
13. Hill SC, Namde M, Dwyer A, Poznanski A, Canna S, Goldbach-Mansky R. Arthropathy of neonatal onset multisystem inflammatory disease (NOMID/CINCA). Pediatr Radiol 2007;37:145–52.
14. Mackie EJ, Tatarczuch L, Mirams M. The skeleton: a multifunctional complex organ. The growth plate chondrocyte and endochondral ossification. J Endocrinol 2011;211:109–21.
15. Goldring MB, Tsuchimochi K, Ijiri K. The control of chondrogenesis. J Cell Biochem 2006;97:33–44.
16. Bonar SL, Brydges SD, Mueller JL, McGeough MD, Pena C, Chen D, et al. Constitutively activated NLRP3 inflammasome causes inflammation and abnormal skeletal development in mice. PloS One 2012;7:e35979.
17. Tanaka T, Takahashi K, Yamane M, Tomida S, Nakamura S, Oshima K, et al. Induced pluripotent stem cells from CINCA syndrome patients as a model for dissecting somatic mosaicism and drug discovery. Blood 2012;120:1299–308.
18. Umeda K, Zhao J, Simmons P, Stanley E, Elefanty A, Nakayama N. Human chondrogenic paraxial mesoderm, directed specification and prospective isolation from pluripotent stem cells. Sci Rep 2012;2:455.
19. Nasu A, Ikeya M, Yamamoto T, Watanabe A, Jin Y, Matsumoto Y, et al. Genetically matched human iPS cells reveal that propensity for cartilage and bone differentiation differs with clones, not cell type of origin. PloS One 2013;8:e53771.
20. Sakai H, Okafuji I, Nishikomori R, Abe J, Izawa K, Kambe N, et al. The CD40-CD40L axis and IFN-γ play critical roles in Langhans giant cell formation. Int Immunol 2012;24:5–15.
21. Aoyama T, Okamoto T, Nagayama S, Nishijo K, Ishibe T, Yasura K, et al. Methylation in the core-promoter region of the chondromodulin-I gene determines the cell-specific expression by regulating the binding of transcriptional activator Sp3. J Biol Chem 2004;279:28789–97.
22. Ushita M, Saito T, Ikeda T, Yano F, Higashikawa A, Ogata N, et al. Transcriptional induction of SOX9 by NF-κB family member RelA in chondrogenic cells. Osteoarthritis Cartilage 2009;17:1065–75.
23. Kajita Y, Kato T Jr, Tamaki S, Furu M, Takahashi R, Nagayama S, et al. The transcription factor Sp3 regulates the expression of a metastasis-related marker of sarcoma, actin filament-associated protein 1-like 1 (AFAP1L1). PloS One 2013;8:e49709.
24. Sandelin A, Alkema W, Engstrom P, Wasserman WW, Lenhard B. JASPAR: an open-access database for eukaryotic transcription factor binding profiles. Nucleic Acids Res 2004;32:D91–4.
25. Saito M, Fujisawa A, Nishikomori R, Kambe N, Nakata-Hizume M, Yoshimoto M, et al. Somatic mosaicism of CIAS1 in a patient with chronic infantile neurologic, cutaneous, articular syndrome. Arthritis Rheum 2005;52:3579–85.
26. Saito M, Nishikomori R, Kambe N, Fujisawa A, Tanizaki H, Takeichi K, et al. Disease-associated CIAS1 mutations induce monocyte death, revealing low-level mosaicism in mutation-negative cryopyrin-associated periodic syndrome patients. Blood 2008;111:2132–41.
27. Aksentijevich I, Nowak M, Mallah M, Chae JJ, Watford WT, Hofmann SR, et al. De novo CIAS1 mutations, cytokine activation, and evidence for genetic heterogeneity in patients with neonatal-onset multisystem inflammatory disease (NOMID): a new member of the expanding family of pyrin-associated autoinflammatory diseases. Arthritis Rheum 2002;46:3340–8.
28. Akiyama H, Lefebvre V. Unraveling the transcriptional regulatory machinery in chondrogenesis. J Bone Miner Metab 2011;29:390–5.
29. Kim Y, Murao H, Yamamoto K, Deng JM, Behringer RR, Nakamura T, et al. Generation of transgenic mice for conditional overexpression of Sox9. J Bone Miner Metab 2011;29:123–9.
30. Cucchiarini M, Orth P, Madry H. Direct rAAV SOX9 administration for durable articular cartilage repair with delayed terminal differentiation and hypertrophy in vivo. J Mol Med (Berlin) 2013;91:625–36.
31. Cucchiarini M, Thurn T, Weimer A, Kohn D, Terwilliger EF, Madry H. Restoration of the extracellular matrix in human

osteoarthritic articular cartilage by overexpression of the transcription factor SOX9. Arthritis Rheum 2007;56:158–67.
32. Tew SR, Li Y, Pothacharoen P, Tweats LM, Hawkins RE, Hardingham TE. Retroviral transduction with SOX9 enhances re-expression of the chondrocyte phenotype in passaged osteoarthritic human articular chondrocytes. Osteoarthritis Cartilage 2005;13:80–9.
33. Carroll SH, Ravid K. Differentiation of mesenchymal stem cells to osteoblasts and chondrocytes: a focus on adenosine receptors. Expert Rev Mol Med 2013;15:e1.
34. Huang W, Zhou X, Lefebvre V, de Crombrugghe B. Phosphorylation of SOX9 by cyclic AMP-dependent protein kinase A enhances SOX9's ability to transactivate a Col2a1 chondrocyte-specific enhancer. Mol Cell Biol 2000;20:4149–58.
35. Tsuda M, Takahashi S, Takahashi Y, Asahara H. Transcriptional co-activators CREB-binding protein and p300 regulate chondrocyte-specific gene expression via association with Sox9. J Biol Chem 2003;278:27224–9.
36. Yoon YM, Oh CD, Kang SS, Chun JS. Protein kinase A regulates chondrogenesis of mesenchymal cells at the post-precartilage condensation stage via protein kinase C-α signaling. J Bone Miner Res 2000;15:2197–205.
37. Almeida MQ, Tsang KM, Cheadle C, Watkins T, Grivel JC, Nesterova M, et al. Protein kinase A regulates caspase-1 via Ets-1 in bone stromal cell-derived lesions: a link between cyclic AMP and pro-inflammatory pathways in osteoblast progenitors. Hum Mol Genet 2011;20:165–75.
38. Lee GS, Subramanian N, Kim AI, Aksentijevich I, Goldbach-Mansky R, Sacks DB, et al. The calcium-sensing receptor regulates the NLRP3 inflammasome through Ca^{2+} and cAMP. Nature 2012;492:123–7.
39. Rossol M, Pierer M, Raulien N, Quandt D, Meusch U, Rothe K, et al. Extracellular Ca^{2+} is a danger signal activating the NLRP3 inflammasome through G protein-coupled calcium sensing receptors. Nat Commun 2012;3:1329.
40. Barberi T, Willis LM, Socci ND, Studer L. Derivation of multipotent mesenchymal precursors from human embryonic stem cells. PLoS Med 2005;2:e161.
41. Kawaguchi J, Mee PJ, Smith AG. Osteogenic and chondrogenic differentiation of embryonic stem cells in response to specific growth factors. Bone 2005;36:758–69.
42. Zur Nieden NI, Kempka G, Rancourt DE, Ahr HJ. Induction of chondro-, osteo- and adipogenesis in embryonic stem cells by bone morphogenetic protein-2: effect of cofactors on differentiating lineages. BMC Dev Biol 2005;5:1.

STEM CELLS TRANSLATIONAL MEDICINE®

PLURIPOTENT STEM CELLS

Pluripotent Cell Models of Fanconi Anemia Identify the Early Pathological Defect in Human Hemoangiogenic Progenitors

NAOYA M. SUZUKI,[a] AKIRA NIWA,[a] MIHARU YABE,[b] ASUKA HIRA,[c] CHIHIRO OKADA,[d,e] NAOKI AMANO,[d] AKIRA WATANABE,[d] KEN-ICHIRO WATANABE,[f,g] TOSHIO HEIKE,[f] MINORU TAKATA,[c] TATSUTOSHI NAKAHATA,[a] MEGUMU K. SAITO[a]

Key Words. Induced pluripotent stem cells • Fanconi anemia • Hematopoietic progenitors • Differentiation • Transcription factors

ABSTRACT

Fanconi anemia (FA) is a disorder of genomic instability characterized by progressive bone marrow failure (BMF), developmental abnormalities, and an increased susceptibility to cancer. Although various consequences in hematopoietic stem/progenitor cells have been attributed to FA-BMF, the quest to identify the initial pathological event is still ongoing. To address this issue, we established induced pluripotent stem cells (iPSCs) from fibroblasts of six patients with FA and *FANCA* mutations. An improved reprogramming method yielded iPSC-like colonies from all patients, and iPSC clones were propagated from two patients. Quantitative evaluation of the differentiation ability demonstrated that the differentiation propensity toward the hematopoietic and endothelial lineages is already defective in early hemoangiogenic progenitors. The expression levels of critical transcription factors were significantly downregulated in these progenitors. These data indicate that the hematopoietic consequences in FA patients originate from the early hematopoietic stage and highlight the potential usefulness of iPSC technology for elucidating the pathogenesis of FA-BMF. STEM CELLS TRANSLATIONAL MEDICINE *2015;4:1–6*

Departments of [a]Clinical Application and [d]Reprogramming Science, Center for Induced Pluripotent Stem Cell Research and Application, and [c]Laboratory of DNA Damage Signaling, Department of Late Effects Studies, Radiation Biology Center, Kyoto University, Kyoto, Japan; [b]Department of Cell Transplantation and Regenerative Medicine, Tokai University School of Medicine, Isehara, Japan; [e]Mitsubishi Space Software Co., Ltd., Amagasaki, Japan; [f]Department of Pediatrics, Kyoto University Graduate School of Medicine, Kyoto, Japan; [g]Department of Hematology and Oncology, Shizuoka Children's Hospital, Shizuoka, Japan

Correspondence: Megumu K. Saito, M.D., Ph.D., 53 Shogoin-Kawahara-cho, Sakyo-ku, Kyoto 606-8507, Japan. Telephone: 81-75-366-7089; E-Mail: msaito@cira.kyoto-u.ac.jp

Received September 20, 2014; accepted for publication January 7, 2015.

1066-5099/2015/$20.00/0

http://dx.doi.org/10.5966/sctm.2013-0172

INTRODUCTION

Fanconi anemia (FA) is a disorder of genomic instability characterized by progressive bone marrow failure (BMF), developmental abnormalities, and an increased susceptibility to cancer [1–3]. The responsible genes form a common DNA repair network referred to as the FA pathway [4]. The FA pathway has been considered to be involved in repair of DNA interstrand cross-links (ICLs) [1–4]. The FA pathway is activated by ICL damage, leading to the monoubiquitination of Fanconi anemia, complementation group D2 (FANCD2) and Fanconi anemia, complementation group I (FANCI) proteins (ID complex) by FA core E3 ligase complex. The monoubiquitinated ID complex is then loaded on damaged chromatin and mediates homologous recombination and translesion synthesis. Although accelerated apoptosis and cell cycle arrest in hematopoietic stem/progenitor cells have been associated with BMF in patients with FA [5], precisely how and when the initial event that causes this consequence occurs have been unclear. Recent reports have indicated that the fate of hematopoietic progenitors has already been determined during fetal liver hematopoiesis both in humans and in mouse models of FA [5, 6]. However, tracing the earlier developmental events to capture the initial event is both technically and ethically impossible at present in humans.

Induced pluripotent stem cells (iPSCs) established from patients with FA may be useful to address these issues because, in combination with a proper hematopoietic differentiation system, iPSCs can enable evaluation of the human developmental stages [7, 8]. In this study, we established iPSCs from patients with FA and found that their differentiation propensity toward the hematopoietic lineage was already defective in the early hemoangiogenic progenitor stage. This report shows the possibility that the hematopoietic consequences in patients with FA originate at the earliest hematopoietic stage.

MATERIALS AND METHODS

Detailed methods are included in the supplemental online data.

Study Ethics

This study was approved by the ethics committees of Kyoto University and Tokai University, and informed consent was obtained from the